Journal of The Electrochemical Society, **156** (8) G89-G96 (2009)
0013-4651/2009/156(8)/G89/8/$25.00 © The Electrochemical Society

Atomic Layer Deposition of Hafnium Silicate Thin Films Using Tetrakis(diethylamido)hafnium and Tris(2-methyl-2-butoxy)silanol

Jian Liu,[a] William N. Lennard,[a,z] Lyudmila V. Goncharova,[a] Dolf Landheer,[b,*] Xiaohua Wu,[b] Simon A. Rushworth,[c] and Anthony C. Jones[d]

[a]*Department of Physics and Astronomy, University of Western Ontario, London, Ontario N6A 3K7, Canada*
[b]*Institute for Microstructural Sciences, National Research Council of Canada, Ottawa, Ontario K1A 0R6, Canada*
[c]*SAFC Hitech Limited, Wirral CH62 3QF, United Kingdom*
[d]*Department of Chemistry, University of Liverpool, Liverpool L69 7ZD, United Kingdom*

Hafnium silicate films were grown by atomic layer deposition using the liquid precursors tetrakis(diethylamido)hafnium (TDEAH) and tris(2-methyl-2-butoxy)silanol, $[CH_3CH_2C(CH_3)_2O]_3SiOH$ (TMBS). Using in situ ellipsometry, ex situ high resolution transmission electron microscopy (HRTEM), medium energy ion scattering (MEIS), and X-ray photoelectron spectroscopy (XPS), the details of the film thickness and composition were examined as functions of both the substrate temperature and silanol pulse time. Both HRTEM and MEIS measurements revealed that the films comprised two layers, with the surface layer containing more Hf than the layer in contact with the substrate. A self-limiting growth with a rate ~1 ML/cycle was observed only after several initial cycles, a behavior that is ascribed to the chemistry of the initial Si substrate surface. Hf 4f XPS confirmed that the films were stoichiometric $Hf_xSi_{1-x}O_2$ throughout despite the nonconstant Hf concentration with depth. A reaction mechanism between TDEAH and TMBS is proposed.
 [DOI: 10.1149/1.3137053]

Manuscript submitted November 21, 2008; revised manuscript received March 20, 2009. Published May 21, 2009.

As the feature size of integrated circuits continues to shrink, research has intensified to find a suitable substitute gate dielectric material for SiO_2 or SiO_xN_y. Attention is now focused on hafnium-based materials, in particular, Hf silicates. Among the variety of techniques available for the fabrication of such high-κ dielectric films, three variants can be identified: (*i*) Physical vapor deposition,[1,2] (*ii*) metallorganic chemical vapor deposition,[3,4] and (*iii*) atomic layer deposition (ALD).[5-11] The most promising of these methods appears to be ALD wherein a series of self-limiting surface reactions occurring at relatively low temperatures have been used to produce amorphous, uniform, conformal films of controlled thickness with good interface properties and low contaminant levels.[12] $HfCl_4$ has been widely employed as a precursor in the ALD of Hf silicate films.[5-7] However, Cl impurities are often found in the resultant films, and corrosive halide by-products can be detrimental both to the film and to the deposition equipment. Hausmann et al. introduced the possibility of using Hf alkylamides as precursors for HfO_2 thin-film ALD because $Hf(NMe_2)_4$, $Hf(NMeEt)_4$, and $Hf(NEt_2)_4$ were highly reactive with hydroxylated surfaces.[12]

In this work, the ALD growth of Hf silicate films using an alternating sequence of tetrakis(diethylamido)hafnium $[Hf(NEt_2)_4]$ (TDEAH) and tris(2-methyl-2-butoxy)silanol ($[CH_3CH_2C(CH_3)_2O]_3SiOH$) (TMBS) precursors is reported where both precursor molecules are larger than those used by Gordon et al.[8] The most established ALD processes use H_2O or O_3 exposure as the oxygen source. As a result a detectable amount of SiO_2 has often been found at the dielectric/Si interface upon completion of the film growth. In this work, TMBS is used both as an oxygen source and as a Si precursor. The resultant film structure and composition were studied as a function of substrate temperature and TMBS pulse times, thereby establishing an effective ALD temperature window. In situ ellipsometry and both in situ and ex situ X-ray photoelectron spectroscopies (XPSs) were applied to monitor film thickness and composition, respectively. An online residual gas analyzer (RGA) was used to continuously detect gaseous species present during the growth process. The depth distribution of Hf was determined from ex situ medium energy ion scattering (MEIS) measurements and high resolution transmission electron microscopy (HRTEM). A possible reaction mechanism between the TDEAH and TMBS precursors is suggested.

Experimental

Hafnium silicate films were grown on p-type Si(001) wafers in a cold-wall ($T < 100°C$) ALD chamber. The silicon wafers were cleaned by the RCA method with a HF dip as the last step and inserted through a load lock into the ALD chamber. Before deposition, the substrates were oxidized for 300 s in oxygen at 500°C. TDEAH, a liquid at room temperature, was used as the Hf precursor. Instead of the oxidation step with H_2O or O_3, TMBS was used as both the silicon precursor and the oxygen source. A liquid injection pump delivered TDEAH dissolved as a 0.1 M solution in octane into a vaporizer which was heated to 140°C. The vaporized hafnium precursor was introduced into the deposition chamber via Ar carrier gas. The silicon precursor was stored in a bubbler and introduced into the chamber by flowing N_2 gas through the bubbler, heated to 50°C. N_2 was flowing into the chamber at all times, and the two precursor pulses were separated by a nitrogen purge step. A differentially pumped RGA mass spectrometer connected to the deposition chamber monitored the partial pressures of different gases involved in the film growth process. The thickness increase in the film was monitored by an in situ ellipsometer (J.A. Woollam, M2000). Following the film deposition, both in situ and ex situ XPS spectra were recorded to ascertain the chemical state of the constituent species in the films. ⟨011⟩ cross-sectional transmission electron microscope (TEM) samples were prepared following standard dimpling and ion-milling procedures. The TEM samples were characterized by HRTEM and high angle annular dark-field scanning transmission electron microscopy (HAADF-STEM) in a JEOL JEM-2100F TEM operating at 200 kV.

To obtain compositional depth profiles, MEIS experiments were performed using incident 95 keV hydrogen ions accelerated by a 1.7 MV Tandetron accelerator, where the samples were transferred in air from the growth chamber into a different ultrahigh vacuum (UHV) chamber. MEIS has been used previously for depth distribution measurements of thin HfO_2 films.[13-16] In the present investigation, a double alignment (channeling/blocking) geometry ($\langle 101\rangle_{in}$ and $\langle 10\bar{1}\rangle_{out}$) was employed to collect the scattered ions in a two-dimensional detector. The MEIS technique is a high resolution version of Rutherford backscattering, i.e., elastic scattering using $^1H^q$

* Electrochemical Society Active Member.
z E-mail: wlennard@uwo.ca

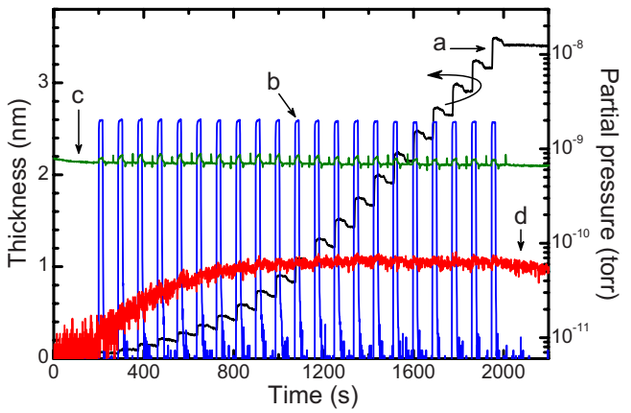

Figure 1. (Color online) Growth process of a film deposited at 350°C: (a) film thickness measured by ellipsometry, (b) Ar partial pressure, (c) N_2 partial pressure, and (d) H_2O partial pressure.

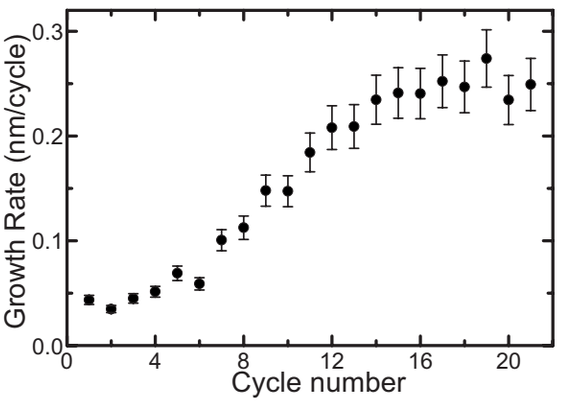

Figure 2. Growth rate as a function of cycle number for the growth shown in Fig. 1.

($q = \pm 1$) ions instead of the usual $^4He^{q+}$ ions. The high energy resolution was provided by the toroidal electrostatic analyzer used to energy analyze the scattered particle flux. The equipment description and experimental setup were described in detail by Kim et al.[17] The depth profiles were then extracted from simulations of the elastically scattered energy distributions of ions with assumptions concerning the physical density of the film because all ion-beam analysis techniques are dependent on ion-stopping powers and yield results for areal densities, i.e., atom/cm^2. The depth resolution at the surface for our system was 0.7 nm, which deteriorated with increasing depth due to energy-loss straggling. The MEIS data represent an average over the ion-beam footprint size, i.e., ~0.1 mm^2, which makes their interpretation difficult with regard to interface or surface roughness or compositional gradients. Despite the foregoing caveats, the MEIS data yield absolute areal densities for C, O, Si, and Hf.

Results

Figure 1 shows the film thickness and partial pressures of Ar, N_2, and H_2O as a function of time during the ALD growth of a Hf silicate film at 350°C. Because refractive indexes for ultrathin films are not available, ellipsometry cannot accurately measure the thickness for films with a thickness of <10 nm.[10] However, in the ultrathin-film regime, in situ ellipsometry can still be used to monitor changes in film thickness as the growth proceeds: We will therefore for now assign a relative uncertainty of ±10% to film thickness values from ellipsometry. The pressure values (shown on the vertical axis at the right) are approximately 4 orders of magnitude lower than the true partial pressures inside the deposition chamber due to the presence of an orifice between the chamber and the RGA filament. Figure 2 shows the growth rate as a function of cycle number: The growth rate of the first several cycles is small, 0.05 nm/cycle initially as the film thickness increases approximately parabolically with cycle number. This behavior indicates that there is an effective barrier for TDEAH and TMBS to adsorb onto the initial silicon suboxide surface. The growth rate increases gradually with cycle number and finally reaches a stable value after 14 cycles. Figure 1 shows the concomitant increase in water pressure after the commencement of film deposition. Therefore, H_2O is a reaction product because no water source is involved in the reaction between TDEAH and TMBS. Figure 3 shows the growth details for a single cycle (number 15) of the deposition, corresponding to the linear range of the growth curve shown in Fig. 1 (thickness from ellipsometry). After the introduction of TDEAH into the growth chamber, TDEAH molecules saturate the surface quickly (within 3–4 s). Additional exposure to the TDEAH precursor using a longer pulse time results in no further growth of the film. However, it takes a finite time for the Si precursor, TMBS, to react with the surface. Figure 3 shows that the thickness of the film has equilibrated (i.e., ceases to change) after 25 s exposure to TMBS even though TMBS vapor is still present and available in the chamber. The ellipsometry trace in Fig. 3 clearly shows the self-limiting behavior of both the TDEAH and TMBS precursors corresponding to the 15th growth cycle.

To confirm that the ellipsometric data provided a valid metric for film thickness, several samples were prepared following a specific number of cycles, and the samples were then examined via HRTEM to establish an independent measure of film thickness. Figure 4 shows the film thicknesses determined from both TEM and ellipsometry. Linear fits to both sets of data produce a positive abscissa intercept which confirms the initial nonlinear behavior described earlier. The slopes agree within 10%: 0.33 ± 0.02 nm/cycle for the TEM data and 0.31 ± 0.03 nm/cycle for the ellipsometric data. The thicknesses determined from TEM were always larger than those derived from ellipsometric data. With a 10% relative uncertainty for the ellipsometric values and an absolute uncertainty of 5% for the TEM measurements, the ratio of TEM/ellipsometric thickness was 1.34 ± 0.15. Additional confirmation of absolute film thickness is expected via MEIS data.

The substrate temperature (T_{sub}) was varied in the range 200–375°C. Figure 5 shows a portion of the growth cycle for T_{sub} = 200°C. Here, even after 100 s of TMBS exposure, the reaction between the precursors is not yet complete as the film thickness is still changing.

Figure 6 shows the growth rate as a function of TMBS pulse time at three different substrate temperatures in the range 250–350°C. At T_{sub} = 350°C, 25 s of TMBS pulse time saturates the surface. At

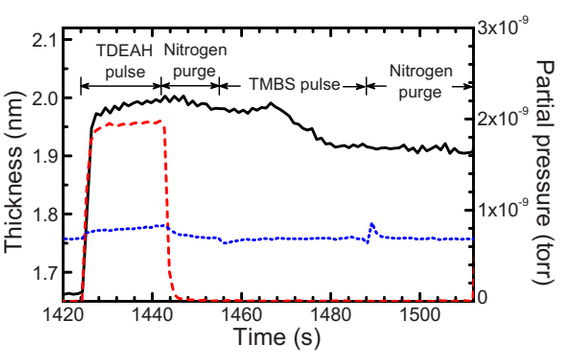

Figure 3. (Color online) Details of the variation in the film thickness and gaseous partial pressures during the 15th growth cycle of the deposition shown in Fig. 1 (at 350°C): film thickness (solid curve) measured by ellipsometry, Ar partial pressure (dashed curve), and N_2 partial pressure (dotted curve). TDEAH is delivered by argon, while TMBS is delivered by nitrogen.

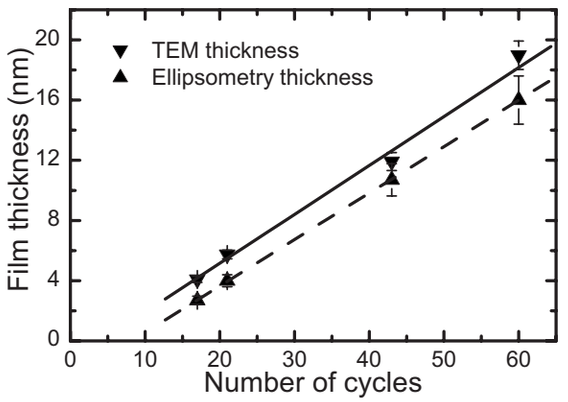

Figure 4. Film thickness as a function of the number of cycles. Slope of linear fit (solid line) to TEM data = 0.33 ± 0.02 nm/cycle and slope of linear fit (dashed line) to ellipsometry data = 0.31 ± 0.03 nm/cycle.

300°C, 40 s of TMBS pulse time is required. At 250°C, even 80 s of TMBS pulse time is insufficient to achieve a saturated growth rate. When the half-cycle TMBS pulse time is not long enough at a low substrate temperature, a doubling of the nitrogen flow rate through the TMBS bubbler resulted in no further growth of the film. In these experiments, the reaction time rather than precursor volume is then the crucial variable for the growth at lower temperatures. TDEAH was observed to decompose at T_{sub} = 375°C (data not shown).

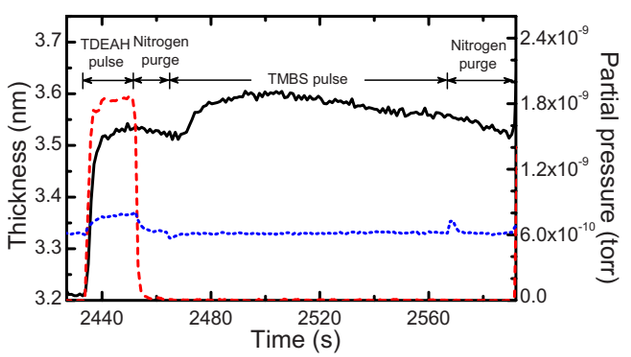

Figure 5. (Color online) One of the growth cycles at T_{sub} = 200°C: film thickness (solid curve) measured by ellipsometry, Ar partial pressure (dashed curve), and N_2 partial pressure (dotted curve).

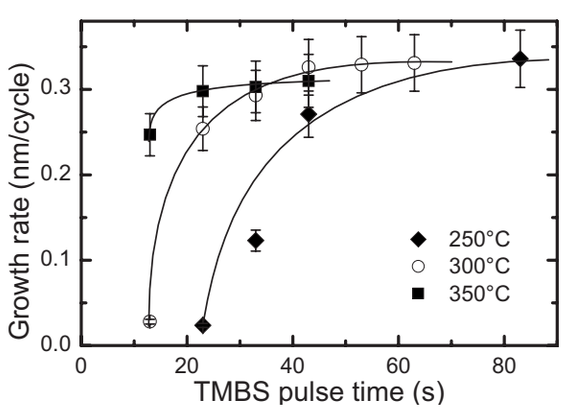

Figure 6. Growth rate as a function of TMBS pulse time for three substrate temperatures (curves are to guide the eyes).

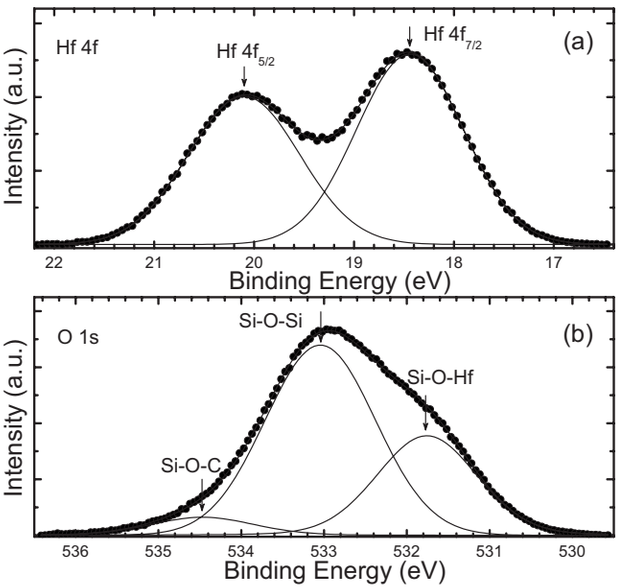

Figure 7. XPS (ex situ) peaks for a film grown at 350°C: (a) Hf 4f and (b) O 1s regions.

Therefore, the temperature window to achieve reproducible ALD growth is 250–350°C using the precursors TDEAH and TMBS.

Both in situ and ex situ XPS analyses were performed for chemical analysis using Mg Kα (1253.6 eV, in situ) and Al Kα (1486.6 eV, ex situ) X-ray sources. For the ex situ data, an X-ray monochromator was used. The photoelectron take-off angle was 45° in both cases. For Si 2p photoelectrons excited by Mg Kα and Al Kα X-rays, the inelastic mean free paths (λ) in SiO_2 are ~2.5 [18] and ~3.0 nm,[19] respectively. The λ value of Si 2p photoelectrons in Hf silicate films is expected to be approximately the same as in SiO_2. In an XPS spectrum, ~95% of the photoelectron yield arises from a depth of ~3λ. Considering the 45° photoelectron take-off angle, the sampling depth in our XPS analyses is therefore ~5.8 nm. The thicknesses of Hf silicate films grown in this study are in the range 4–5 nm (with the exception of those shown in Fig. 4 used to calibrate the length scale). Therefore, the XPS data measure the photoelectron yield for the entire film. This conclusion is supported by the observation of the substrate Si^0 2p XPS signal at 99.3 eV (which is used as a reference).

Figures 7a and b shows the ex situ XPS Hf 4f and O 1s peaks, respectively, for a typical Hf silicate film. The separation between the Hf $4f_{5/2}$ and Hf $4f_{7/2}$ peaks is 1.66 eV, in good agreement with the results of Ulrich et al.[20] In Fig. 7a, the binding energy (BE) and full width at half-maximum of the Hf $4f_{7/2}$ peak are 18.4 and 1.26 eV, respectively. Considering the composition of the specific film [Hf/(Si + Hf) = 0.25] studied here, both values agree very well with the results of Ref. 20 for $Hf_xSi_{1-x}O_2$ films with Hf/(Si + Hf) = 0.25. No Hf–silicide bonding at BE = 14.3 eV or HfO_2 bonding at BE = 17.7 eV [21] was observed.

For the O 1s peaks, the peaks at BEs of 533.0 and 531.8 eV correspond to Si–O–Si and Si–O–Hf bonds, respectively.[22] Their separation is 1.28 eV, in agreement with O'Connor et al.[23] Lao et al.[24] observed an O 1s peak at 535 eV in plasma-enhanced ALD HfO_2 films which they attributed to the Hf–O–C bond. In our case, the O 1s peak at 534.5 eV should originate from the Si–O–C bond, considering the composition of our films and the precursor chemistry.

The in situ and ex situ C 1s peaks are shown in Fig. 8. Figure 8a shows C–O, C–C, [25] and C–Hf[26] bonds in the in situ XPS spectrum. The C 1s peak at a BE of 281.0 eV is attributed to the C–Hf bond.[26] After atmospheric exposure, the C–Hf bond disappeared, indicating

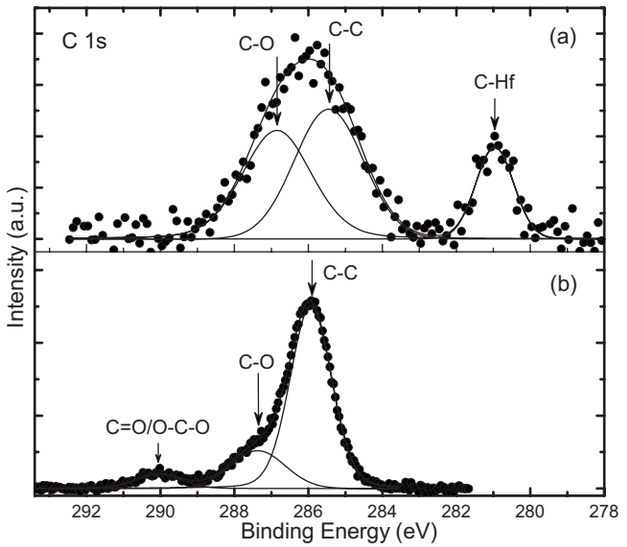

Figure 8. C 1s XPS peaks: (a) in situ and (b) ex situ after several days of exposure to air.

that the Hf carbide was oxidized upon exposure to air. Thus, the observation of the C = O or O–C–O [25] bonds and the greatly increased C–C bonds in the ex situ XPS spectrum is due to carbon contamination which is again caused by exposure to air. The slight shift between the C–C peaks between in situ and ex situ spectra is probably due to a small calibration difference for the two XPS systems because the observed 1.4 eV separation of the C–O and C–C peaks is the same for both the in situ and ex situ spectra.

Figures 9a and b show the bright-field HRTEM and dark-field HAADF-STEM images, respectively, for the as-deposited film grown at 350°C. In the bright-field image, the darker area near the surface indicates a region of higher Hf concentration relative to the brighter area. In the dark-field image, the contrast is more sensitive to the atomic number of the film constituent atoms, confirming the Hf-rich surface region of the film apparent in Fig. 9a.

Figure 10 shows the MEIS experimental data and simulation results for the same sample shown in Fig. 9. The simulations are provided by a computer fitting program (derived from the Quark series[27] of elastic-scattering simulations) where separate discrete layers are assumed to have abrupt boundaries. The arrows indicate the surface-edge position of Hf, Si, O, and C, respectively, because elastic-scattering surface energies are dependent only on the scattering angle and the mass ratio, M_2/M_1 ($M_1 = 1$ for protons). Figure 10b shows the composition profile extracted from the simulation, and Table I lists the parameters used for each layer in the MEIS model. The top layer, considering its thickness, is just adventitious carbon contamination either from atmospheric exposure before the MEIS experiments or resulting from ion-beam-induced hydrocarbon cracking even in a UHV environment. The second layer is a Hf silicate layer corresponding to the Hf-rich layer observed in the bright-field TEM image; see Fig. 9a. The third layer is a Si suboxide layer containing a small Hf concentration corresponding to the Hf-deficient layer in Fig. 9a. However, the detailed composition of this layer is still an open question because it is not easy for MEIS to differentiate the Si atoms located at the bottom of the film from those Si atoms located in the substrate surface region.

The film composition was calculated from both the in situ XPS spectra and the MEIS data. When calculating the film composition from the MEIS data, the Hf-deficient layer is excluded because the Si signal from the substrate is not adequately resolved from the Si signal for the interface layer. This restriction is not overly restrictive because for the results shown in Table I, the Hf-rich layer (i.e., layer 2) contains ~87% of the total Hf areal density. In the MEIS experi-

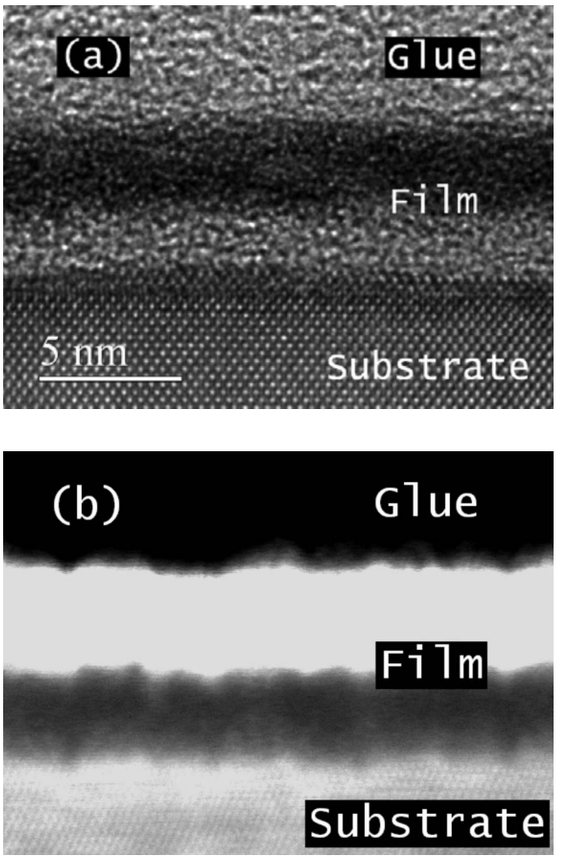

Figure 9. (a) HRTEM and (b) HAADF-STEM images for as-deposited film at 350°C.

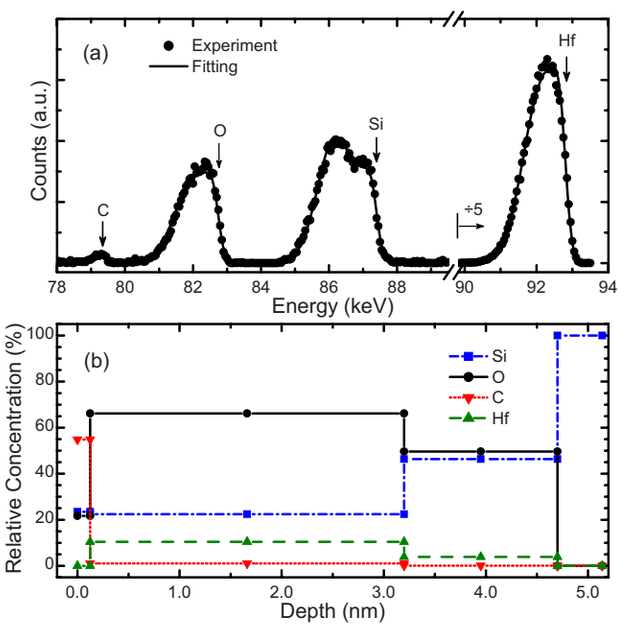

Figure 10. (Color online) (a) MEIS spectrum for the sample shown in Fig. 9. The arrows indicate the positions of surface edges of Hf, Si, O, and C, respectively. (b) The depth profiles of Hf, Si, O, and C extracted from a fit to the spectrum shown in (a).

Table I. Parameters derived from a fit to the MEIS spectrum shown in Fig. 10a.

MEIS model						
			Concentration (atom %)			
Layer	Thickness (nm)	Density (g/cm^3)	C	Hf	Si	O
1	0.12	2.7	55	0	23	22
2	3.08	3.6	1.0	10	22	66
3	1.50	2.3	0.10	3.9	46	50

ment, a nitrogen (M = 14) peak is not observed, which indicates that N has a low concentration in the film. Because of the extensive energy width of the oxygen (M = 16) peak, signals from N atoms located at the surface and O atoms located at some depth into the film will overlap.

Table II shows film composition as a function of deposition temperature and TMBS pulse time for a variety of films. The Hf/(Si + Hf) ratios derived from MEIS measurements are 3–5% higher than those measured by XPS, which probably results from the exclusion of the Hf-deficient layer from the MEIS calculations. Table II shows that for the temperature range 200–350°C, the film composition depends mainly on the deposition temperature and only slightly on the TMBS pulse time. As the substrate temperature increases, the Hf concentration depends only weakly on temperature in a nonmonotonic manner. From the XPS data, the C content is highest at lower temperatures, amounting to a few percent in all cases. In contrast, the N content is small, ~1%, at all temperatures.

Reaction Mechanism

The starting surface of the Si substrate is SiO_x bonded after oxidation. It is not easy for TDEAH or TMBS to adsorb on an oxygen-terminated Si surface due to a dearth of –OH sites. Thus the growth rate for the first several cycles is low (Fig. 2). When the film growth enters a stable regime, after the introduction of the Hf precursor, each TDEAH molecule reacts with two surface hydroxyl groups and eliminates two diethylamine molecules (Fig. 11a), which is the same reaction mechanism between hafnium alkylamide and surface hydroxyl groups proposed by Liu et al.[28] The TMBS molecule contains a hydroxyl group. In the subsequent half-cycle TMBS pulse, the hydroxyl groups in the TMBS molecules cleave the Hf–N bond on

Table II. Film composition measured by MEIS and from in situ XPS data.

Sample no.	T_{sub} (°C)	TMBS pulse time per cycle (s)	Composition (atom %) (MEIS) Hf	Si	O	C	Hf/(Si + Hf)	Composition (atom %) (in situ XPS) Hf	Si	O	C	N	Hf/(Si + Hf)
1368	350	13	9.7	21	62	6.7	0.31	7.1	21	67	3.8	1.1	0.25
1369	350	23	8.9	22	64	4.3	0.29	6.6	21	68	3.4	1.0	0.24
1371	350	33	8.9	23	66	2.9	0.28	6.9	22	67	3.3	1.0	0.24
1370	350	43	8.8	23	65	3.9	0.28	6.3	22	68	2.8	0.93	0.22
1373	300	23	9.4	22	63	4.8	0.29	6.8	20	67	4.4	1.4	0.25
1372	300	33	8.9	22	64	4.8	0.29	6.4	21	67	5.0	1.2	0.24
1374	300	43	8.2	22	60	9.5	0.27	6.2	21	68	3.8	1.0	0.23
1351	300	53	8.5	23	65	4.0	0.27	6.4	22	68	2.8	0.92	0.22
1352	300	63	8.3	23	63	5.7	0.26	6.2	22	68	3.2	0.96	0.22
1362	250	33	11	18	60	11	0.37	7.5	18	63	9.1	1.9	0.29
1366	250	43	11	20	64	4.7	0.35	8.1	19	66	5.7	1.4	0.30
1356	250	83	9.5	21	63	5.8	0.31	7.0	20	67	4.5	1.1	0.26
1367	200	103	12	19	62	6.0	0.38	8.2	18	65	7.1	1.4	0.31

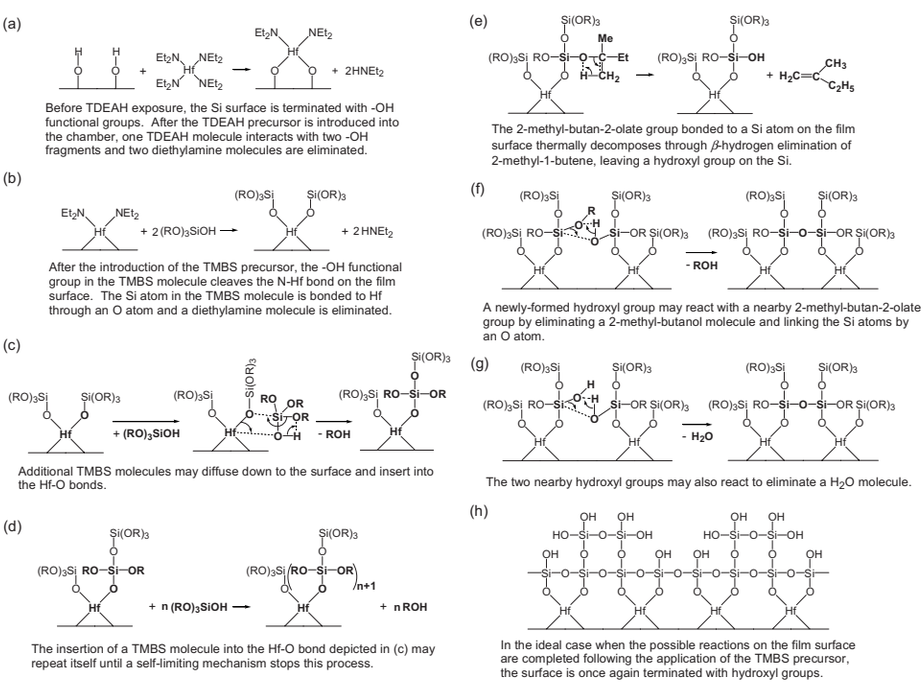

Figure 11. Proposed reaction mechanism between TDEAH and TMBS. Me ↔ [−CH_3] group, Et ↔ [−C_2H_5] group, and R ↔ [−$C(CH_3)_2C_2H_5$] group.

the chemisorbed TDEAH and produce diethylamine molecules as a by-product (Fig. 11b). This reaction step is similar to reaction between surface-chemisorbed $Hf(NMeEt)_4$ and water.[28] Therefore after application of the TMBS precursor, each Hf atom on the surface can bond to two Si atoms via oxygen atoms because there is only one hydroxyl group in each TMBS molecule. Additional TMBS molecules can diffuse down to the surface and insert into the Hf–O bonds by eliminating 2-methyl-2-butanol molecules (Fig. 11c) because the catalytic activity of Hf atoms lowers the activation energy of this reaction.[29] This reaction may repeat itself as long as the TMBS molecules can diffuse through the precursor ligands and reach the Hf–O bonds at the surface (Fig. 11d).[29]

The self-limiting mechanism is achieved by the cross-linking of the Si atoms through O atoms. The 2-methyl-butan-2-olate groups bonded to Si atoms on the surface undergo thermal decomposition through β-hydrogen elimination of 2-methyl-1-butene (Fig. 11e), leaving hydroxyl groups on the silicon (similar to Scheme 1E, Ref. 29). Alternatively, the C–C bond in the 2-methyl-butan-2-olate group can break instead of the C–O bond. As a result, C will be left in the films as an impurity. This explanation is supported by the observed O 1s XPS peak which corresponds to Si–O–C bonding (Fig. 7b). A newly formed hydroxyl group may react with a nearby 2-methyl-butan-2-olate group by eliminating a 2-methyl-2-butanol molecule and link the silicon atoms by an oxygen atom (Fig. 11f) (similar to Scheme 1F, Ref. 29). The cross-linking between silicon atoms may also be achieved by elimination of H_2O between two adjacent hydroxyl groups (Fig. 11g) (similar to Scheme 1G, Ref. 29). The increase in water pressure observed by the RGA shown in Fig. 1 confirms this reaction step. In the ideal case, given a sufficiently long time interval following the application of TMBS, all the 2-methyl-butan-2-olate groups either decompose to leave hydroxyl groups on the surface or react with the near-surface hydroxyl groups and eliminate 2-methyl-2-butanol molecules. Therefore when the surface is stabilized following a TMBS pulse, it should be terminated with hydroxyl groups, as shown in Fig. 11h.

The reaction between the Hf precursor, TDEAH, and the hydroxyl group occurs rapidly, an observation that explains the sharp thickness increase following the application of TDEAH evident in both Fig. 3 and 5. This reaction step is little affected by substrate temperature. However, the time needed for the TMBS to completely react with the surface is temperature dependent. Obviously, a higher substrate temperature contributes to a decrease in the reaction time.

The linear growth rate (after several initial cycles) observed for the films grown in this study was high, 0.33 (±0.02) nm/cycle according to the TEM thickness calibration. Using the relation that 1 ML $\equiv (N_0\rho/\mathrm{MW})^{-1/3}$, where N_0 is Avogadro's number, MW is the molecular weight, and ρ is the density, we find that 1 ML $\equiv 0.365$ nm for $\rho = 3.6$ g/cm^3 and $Hf/(Si + Hf) = 0.3$. Thus, the linear growth rate shown in Fig. 4 corresponds to 1 ML/cycle within experimental uncertainty. This high growth rate cannot be explained by the traditional ALD theory, wherein the growth rate is usually a fraction of a monolayer per cycle due to steric hindrance of the precursor ligands. The above steps describing the diffusion and insertion of silanol precursor into the Hf–O bond mechanism (Fig. 11c and d) during the application of the silanol precursor can explain the high growth rate observed in this study. This reaction mechanism was proposed by Hausmann et al.,[29] who observed abnormally high growth rates (12 nm/cycle) when using trimethylaluminum and tris(*tert*-butoxy)silanol $[(Bu^tO)_3SiOH]$ to grow $(Al_2O_3)_x$–$(SiO_2)_y$ films by ALD. They concluded that it is the presence of Al atoms that makes the catalytic reaction between the surface Al–O bonds and the silanol precursor $(Bu^tO)_3SiOH$ possible. Therefore, many Si–O layers can be deposited in one $(Bu^tO)_3SiOH$ precursor pulse, resulting in an extremely high growth rate. They also suggested that other metals, such as La, Zr, and Hf, should have a similar catalytic activity. They pointed out that the high growth rate (0.3–0.4 nm/cycle) in their earlier ALD experiment using $Hf(NMe_2)_4$ and $(Bu^tO)_3SiOH$ to grow Hf silicate films[8] may be due to the same reaction mechanism. We noticed that both the Hf and Si precursors used in Ref. 8 are similar to the precursors used in this study, with the latter bulkier. The growth rate and the resulting film composition in Ref. 8 are similar to this study. Although the growth rate in this study is much higher than that of the traditional ALD, it is much lower than that observed in Ref. 29. This result is probably because the volume of the Si precursor used in this study is larger than that used in Ref. 29. The bulkier ligands make the diffusion of TMBS molecules (Fig. 11c and d) more difficult than the diffusion of $(Bu^tO)_3SiOH$ in Ref. 29.

Discussion

For future technology applications using high-κ dielectrics, the thickness required is 3–4 nm, and well-controlled growth rates are preferable for thicknesses <3–5 nm. Given the small gate thickness required, the present data suggest that a different initial Si surface composition, e.g., SiO_xN_y or chemical oxide as shown in Ref. 30, should be investigated to look for linear well-behaved growth with no initial nucleation barrier. Our Hf silicate growth data agree with those of Green et al.,[30] who investigated the ALD growth of HfO_2 films via $H_2O/HfCl_4$ chemistry on several variously prepared Si substrates. For a thermal oxide, 15–25 cycles were required to reach the linear growth stage. Our subsequent investigations involving the ALD growth of Hf silicate films on a thick SC-1 precleaned SiO_2 surface for biomolecular field-effect transistor applications,[31] where linear growth was achieved from the outset, agree with the observations of Green et al.[30] for HfO_2.

The film consists of two layers (Fig. 9): The top layer contains a larger Hf concentration than the layer in contact with the silicon substrate. However, the layer with the smaller Hf concentration cannot be the interface (SiO_x) layer formed initially during substrate oxidation at 500°C for 300 s in an O_2 environment. To confirm this assertion, in situ XPS spectra were recorded for the Si^0 2p signal before and after substrate oxidation. The intensity ratio of the Si^0 2p bulk XPS signal before and after oxidation is $I_{after}/I_{before} = 0.88$. Assuming that the mean free path of Si^0 2p photoelectrons excited by the Mg Kα X-rays in the Si suboxide layer is 2.5 nm (the photoelectron take-off angle is 45°), a thickness of 0.22 nm for the initial suboxide layer can be calculated, a value much smaller than the Hf-deficient layer seen in Fig. 9a. The structure of our film is similar to that observed by Quevedo-Lopez et al.[32] for Hf silicate films grown by reactive sputtering. They argued that the film sublayer closer to the substrate is a Hf-deficient layer or possibly a layer of SiO_2. For our films, both the HRTEM and MEIS results show consistently that the layer closer to the substrate is Hf deficient. As already shown, the interface layer formed by substrate oxidation before film deposition is <0.5 nm. However, from the TEM image, it is difficult to resolve the interface layer from the Hf-deficient layer of the film because the interface layer is extremely thin and there is little contrast between these two layers. The composition of our film follows in the metastable extension of the spinodal of the HfO_2–SiO_2 phase diagram, as suggested in Ref. 33. Possibly the Hf silicate film separates into HfO_2-rich and SiO_2-rich phases, and the existence of the substrate surface drives the HfO_2-rich phase to the surface of the film.[34] Possibly the Hf deficient layer is formed by the diffusion of Hf atoms into the SiO_2 layer at the interface. The interface SiO_2 layer may grow from enhanced catalytic oxidation of the Si surface due to the presence of Hf metals in the Hf silicate film. Further investigations to address this issue are in progress.

In this work, the total film thickness for the growth shown in Fig. 1 is 3.4 nm (from ellipsometry). The asymptotic linear growth rate shown in Fig. 2 (also based on ellipsometry) is 0.25 nm/cycle. If the film growth were linear (i.e., self-limiting) from the outset, then we could calculate that $3.4/0.25 \approx 14$ cycles would be needed to achieve the final thickness. The MEIS data for this same film shown in Table I can be used to determine that the absolute total Hf areal density [where $Hf/(Si + Hf) = 0.3$ and we sum over layers 2 and 3] has a value of 2.2×10^{15} Hf atoms/cm^2 or 1.6×10^{14} Hf atoms/cm^2

cycle for each of the 14 cycles. If each Hf atom is bonded to two surface –OH groups, then the surface concentration of those groups is 3.2×10^{14} cm^{-2}. For the SiO_x thin layer, we can approximate the surface Si atom and therefore –OH group (in Fig. 11h) areal densities using $(N_0\rho/MW)^{2/3}$ where we assume that SiO_2 (MW = 60) and $\rho = 2.3$ g/cm^3, resulting in 4.65×10^{14} cm^{-2}, a value in close agreement with that calculated from the observed thickness and growth rate. This calculation lends support to Fig. 11 of the proposed reaction mechanism described earlier.

The data shown in Fig. 2 reveal an asymptotic growth rate of 0.25 nm/cycle in contrast to the initial growth rate of 0.05 nm/cycle. Thus, only 20% coverage is achieved per cycle in the early stages, and five cycles would be needed to completely cover the surface assuming total utilization of unreacted growth sites and layer-by-layer growth. It is common for ALD growth to result in only partial monolayer growth per cycle during the initial stage due to steric hindrance or a lack of reactive sites or island formation,[30] which then renders the observation of 14 cycles needed to reach linear growth not surprising.

Let us consider in detail the results of Table II with regard to the Hf silicate film constituent concentrations. For all cases shown in this table, the TDEAH absorption half-cycle is long enough to saturate the surface. At all temperatures, the in situ XPS data show that the C content decreases slightly with increasing TMBS pulse times, thereby demonstrating that C contamination in the film can be minimized by assuring that the self-limiting condition is achieved for the silanol precursor. The C–O and C–C XPS peaks were greatly reduced following a rapid in situ thermal anneal in vacuum at 800°C. The total C contamination was then reduced to ~1% after such an annealing step.

The concentration of N in the film can only arise from the TDEAH precursor. The N concentrations observed are all ~1 atom % so long as the TMBS pulse times exceed the saturated value at that T_{sub}. This observation is expected because the N–Hf bond can be easily broken by the –OH functional group; see Fig. 11a and b.

Based on the MEIS composition results, the Hf silicate films are stoichiometric, i.e., $O/(Hf + Si) \approx 2$, within the experimental measurement uncertainties and similar to the results of Gordon et al.[8]

The observed TDEAH pulse time required to achieve saturation was quite short, 3 s. This interval is already short enough to satisfy technology needs during processing and perhaps could have been anticipated based on (*i*) the high reactivity of TDEAH with H_2O, i.e., –OH groups, and (*ii*) the results of Liu et al.,[28] who investigated the Hf precursor pulse time dependence of the growth rate for thin HfO_2 films on Si(100) using tetrakis(ethylmethylamino)hafnium whose molecular size is only slightly smaller than that of TDEAH. The latter group found that the Hf precursor half-cycle reached a self-limiting state for pulse times >0.5 s.

With regard to absolute film thicknesses, the MEIS data require a density value of 3.6 g/cm^3 (see Table I) to facilitate a reasonable comparison of MEIS-derived film thickness with TEM film thickness. Thus, ellipsometric, TEM, and MEIS data give length scales that are self-consistent.

The XPS data yield evidence for Hf–O–Si chemical bonding. Ulrich et al.[20] observed a shift of the Hf 4f XPS line energies to lower BE with increasing Hf content for thick Hf silicate films and near-surface sensitivity ($h\nu \sim 130$ eV), where they reported high resolution XPS results for $Hf/(Si + Hf) = 0.25$, 0.50, 0.85, and 1.00. Interpolating their data, it is expected to find Hf $4f_{7/2}$ at BE = 18.5 eV for $Hf/(Si + Hf) = 0.3$, which is in excellent agreement with the measured value of 18.4 eV; see Fig. 7a. Because the $Hf/(Si + Hf)$ ratios measured for our films are nearly the same for all temperatures, we do not expect nor do we see a shift in the Hf 4f line energies measured for films deposited at different T_{sub} values.

It is tempting to identify layer 3 shown in Table I (thickness of ≈1.5 nm) with the parabolic initial growth region apparent in Fig. 1 before the growth rate per cycle plateaus at a constant value. Such a behavior has been reported for ALD growth of HfO_2 by Green et al.[30] for a specific initial surface condition, i.e., a thin thermal oxide. Such a correlation is not justified based on the measured atom fractions: Specifically, the O/Si atom ratio is ~1 and the amount of Hf in this layer is only 13% of the total Hf in the entire film. Green et al.[30] observed that even when the initial growth rate is sublinear, the stoichiometry of the initial layers is not significantly different from that of the entire film, contrary to our observations; see Table I based on MEIS measurements.

Conclusions

Hf silicate films were grown by the ALD technique using TDEAH and TMBS precursors. The growth rate at different substrate temperatures was studied as a function of TMBS pulse time. At low temperature (e.g., 200°C), the TMBS precursor appears to saturate the surface only after a very long pulse time (>200 s). However, a TMBS pulse time of 25 s is adequate to saturate the surface at 350°C. No evidence of hafnium silicide or hafnium oxide bonding was observed according to in situ XPS spectra. The carbon contamination depends on the substrate temperature and the degree of reaction between TMBS and the substrate surface and can be decreased to ~1 atom % after a short (~1 s) in situ vacuum anneal at 800°C.

The composition of the film depends primarily on the deposition temperature, only slightly on the TMBS pulse time, and not at all on the TDEAH pulse time for acceptably long TDEAH exposures (>3 s). The $Hf/(Si + Hf)$ ratio can be adjusted in the limited range 0.22–0.30 by varying both temperature and TMBS pulse time, and the films were stoichiometric in all cases based on XPS and MEIS data, i.e., the composition was $Hf_xSi_{1-x}O_2$ throughout. In the HR-TEM image, an abrupt interface between the substrate and the Hf silicate film was observed for the as-deposited films. From both the bright- and dark-field HRTEM images, the Hf distribution was not uniform throughout the film. A lower Hf concentration layer was observed near the film–substrate interface. This observation was confirmed by MEIS scattered ion data. The formation mechanism and composition of this layer need further investigation.

Acknowledgments

The authors are grateful for the technical assistance of Les Lebrun, Guy Parent, and Simona Moisa at NRCC and Jack Hendriks at UWO and for the helpful comments from Professor G. M. Bancroft. Financial assistance to W.N.L was provided by NSERC (Canada) in the form of a research grant.

University of Western Ontario assisted in meeting the publication costs of this article.

References

1. G. D. Wilk, R. M. Wallace, and J. M. Anthony, *J. Appl. Phys.*, **89**, 5243 (2001).
2. A. Callegari, E. Cartier, M. Gribelyuk, H. F. Okorn-Schmidt, and T. Zabel, *J. Appl. Phys.*, **90**, 6466 (2001).
3. J. Kim and K. Yong, *J. Cryst. Growth*, **263**, 442 (2004).
4. B. Xia, M. L. Fisher, H. Stemper, and A. Misra, *J. Mater. Res.*, **22**, 1024 (2007).
5. K. Kukli, M. Ritala, M. Leskela, T. Sajavaara, J. Keinonen, D. C. Gilmer, and P. J. Tobin, *Mater. Sci. Eng., B*, **109**, 2 (2004).
6. W. K. Kim, S. W. Rhee, N. I. Lee, J. H. Lee, and H. K. Kang, *J. Vac. Sci. Technol. A*, **22**, 1285 (2004).
7. Z. M. Rittersma, F. Roozeboom, M. A. Verheijen, J. G. M. van Berkum, T. Dao, J. H. M. Snijders, E. Vainonen-Ahlgren, E. Tois, M. Tuominen, and S. Haukka, *J. Electrochem. Soc.*, **151**, C716 (2004).
8. R. G. Gordon, J. Becker, D. Hausmann, and S. Suh, *Chem. Mater.*, **13**, 2463 (2001).
9. Y. Senzaki, S. Park, H. Chatham, L. Bartholomew, and W. Nieveen, *J. Vac. Sci. Technol. A*, **22**, 1175 (2004).
10. J. Kim and K. Yong, *J. Electrochem. Soc.*, **152**, F45 (2005).
11. S. Kamiyama, T. Miura, Y. Nara, and T. Arikado, *Electrochem. Solid-State Lett.*, **8**, G215 (2005).
12. D. M. Hausmann, E. Kim, J. Becker, and R. G. Gordon, *Chem. Mater.*, **14**, 4350 (2002).
13. R. P. Pezzi, P. L. Grande, M. Copel, G. Schiwietz, C. Krug, and I. J. R. Baumvol, *Surf. Sci.*, **601**, 5559 (2007).
14. A. Delabie, R. L. Puurunen, B. Brijs, M. Caymax, T. Conard, B. Onsia, O. Richard, W. Vandervorst, C. Zhao, M. M. Heyns, et al., *J. Appl. Phys.*, **97**, 064104 (2005).

15. J. Kim, S. Kim, H. Kang, J. Choi, H. Jeon, M. Cho, K. Chung, S. Back, K. Yoo, and C. Bae, *J. Appl. Phys.*, **98**, 094504 (2005).
16. S. Sayan, S. Aravamudhan, B. W. Busch, W. H. Schulte, F. Cosandey, G. D. Wilk, T. Gustafsson, and E. Garfunkel, *J. Vac. Sci. Technol. A*, **20**, 507 (2002).
17. J. Kim, W. N. Lennard, C. P. McNorgan, J. Hendriks, I. V. Mitchell, D. Landheer, and J. Gredley, *Curr. Appl. Phys.*, **3**, 75 (2003).
18. R. Flitsch and S. I. Raider, *J. Vac. Sci. Technol.*, **12**, 305 (1975).
19. Z. H. Lu, J. P. McCaffrey, B. Brar, G. D. Wilk, R. M. Wallace, L. C. Feldman, and S. P. Tay, *Appl. Phys. Lett.*, **71**, 2764 (1997).
20. M. D. Ulrich, J. G. Hong, J. E. Rowe, G. Lucovsky, A. S. Y. Chan, and T. E. Madey, *J. Vac. Sci. Technol. B*, **21**, 1777 (2003).
21. M. H. Cho, Y. S. Roh, C. N. Whang, K. Jeong, S. W. Nahm, D. H. Ko, J. H. Lee, N. I. Lee, and K. Fujihara, *Appl. Phys. Lett.*, **81**, 472 (2002).
22. H. D. Kim, Y. Roh, Y. Lee, J. E. Lee, D. Jung, and N. E. Lee, *J. Vac. Sci. Technol. A*, **22**, 1347 (2004).
23. R. O'Connor, G. Hughes, P. A. Glans, T. Learmonth, and K. E. Smith, *Appl. Surf. Sci.*, **253**, 2770 (2006).
24. S. X. Lao, R. M. Martin, and J. P. Chang, *J. Vac. Sci. Technol. A*, **23**, 488 (2005).
25. B. O. Cho, S. Lao, L. Sha, and J. P. Chang, *J. Vac. Sci. Technol. A*, **19**, 2751 (2001).
26. L. Ramqvist, K. Hamrin, G. Johansso, A. Fahlman, and C. Nordling, *J. Phys. Chem. Solids*, **30**, 1835 (1969).
27. The Quark simulation for elastic scattering is available at the website of W. N. Lennard: www.uwo.ca/isw/people. Last accessed May 15, 2009.
28. X. Y. Liu, S. Ramanathan, A. Longdergan, A. Srivastava, E. Lee, T. E. Seidel, J. T. Barton, D. Pang, and R. G. Gordon, *J. Electrochem. Soc.*, **152**, G213 (2005).
29. D. Hausmann, J. Becker, S. L. Wang, and R. G. Gordon, *Science*, **298**, 402 (2002).
30. M. L. Green, M. Y. Ho, B. Busch, G. D. Wilk, T. Sorsch, T. Conard, B. Brijs, W. Vandervorst, P. I. Raisanen, D. Muller, et al., *J. Appl. Phys.*, **92**, 7168 (2002).
31. W. H. Jiang, D. Landheer, G. Lopinski, W. R. McKinnon, A. Rankin, E. Ghias-Begloo, R. Griffin, N. G. Tarr, N. Tait, J. Liu, et al., *ECS Trans.*, **16**(11), 441 (2008).
32. M. A. Quevedo-Lopez, M. El-Bouanani, B. E. Gnade, R. M. Wallace, M. R. Visokay, M. Douglas, M. J. Bevan, and L. Colombo, *J. Appl. Phys.*, **92**, 3540 (2002).
33. S. Stemmer, Z. Q. Chen, C. G. Levi, P. S. Lysaght, B. Foran, J. A. Gisby, and J. R. Taylor, *Jpn. J. Appl. Phys., Part 1*, **42**, 3593 (2003).
34. H. Kim and P. C. McIntyre, *J. Appl. Phys.*, **92**, 5094 (2002).